Available online at www.sciencedirect.com
ScienceDirect
Journal of Magnetic Resonance 187 (2007) 266–276
JMR Journal of Magnetic Resonance
www.elsevier.com/locate/jmr

A low-cost implementation of EPR detection in a dissolution DNP setup

Josef Granwehr *, James Leggett, Walter Köckenberger

Sir Peter Mansfield Magnetic Resonance Centre, School of Physics and Astronomy, University of Nottingham, Nottingham NG7 2RD, UK

Received 24 January 2007; revised 4 May 2007
Available online 24 May 2007

Abstract

The implementation of electron paramagnetic resonance (EPR) detection in a low-temperature dissolution dynamic nuclear polarization (DNP) setup is presented. Using a coil oriented parallel to the static magnetic field, the change of the longitudinal magnetization of free radicals is measured upon resonant irradiation of an amplitude or frequency modulated microwave (mw) field. The absorption EPR spectrum is measured if the amplitude of the mw field is modulated, whilst the first derivative of the spectrum is obtained with frequency modulation. Using a burst of pulses, it is also possible to perform pump–probe experiments such as saturation-recovery or electron–electron double resonance experiments. Furthermore, the magnetization could be monitored in a time-resolved manner during amplitude modulation, thus making it possible to record its transient as it is approaching an equilibrium value. Experimental examples are shown with frozen solutions of trityl radical and TEMPO, two commonly used radicals for dissolution DNP experiments.

PACS: 76.30.−v; 07.55.−w; 76.70.−r; 76.30.Rn

Keywords: Electron paramagnetic resonance; EPR; ESR; Longitudinal detection; W band; Frequency sweep; Dynamic nuclear polarization; Dissolution DNP

1. Introduction

Recent developments of novel instruments and experimental procedures have stimulated a renewed interest in using dynamic nuclear polarization (DNP) to strongly enhance nuclear spin polarization. The dissolution DNP method, whereby a sample of interest is frozen at liquid He temperatures in a mixture containing a free radical at a high concentration, then polarized by saturating the EPR transitions of the radical using a strong microwave (mw) field, and finally brought quickly to ambient temperature by flushing it with hot solvent, has made it possible to use DNP techniques in liquid state NMR studies with polarization values of several tens of percent for ^{13}C [1]. This is several orders of magnitude more than is possible with Overhauser enhancement at room temperature [2]. By performing the DNP process in a different magnet than the NMR experiment, both steps can be optimized independently. This also enables the mixing of the polarized sample with an unpolarized one to investigate molecular dynamics such as binding, or to inject a polarized endogenous substance into an organism as a probe for in vivo studies of metabolic pathways [3]. A different approach to obtain high-resolution liquid-state NMR spectra from strongly polarized spin systems is to perform the DNP step in the same magnet as the subsequent NMR experiment by using a laser to melt the sample after DNP. This technique avoids dilution of the sample and has the additional advantage that the experiment can be repeated multiple times [4]. Because DNP and NMR detection are carried out at the same field strength, a high static magnetic field, which is desirable to achieve high-resolution spectra, requires a high-power mw source operating at frequencies beyond 100 GHz [5]. A similar approach was shown to improve the sensitivity of solid-state NMR experiments. To facili-

* Corresponding author. Fax: +44 115 951 5166.
E-mail address: josef.granwehr@nottingham.ac.uk (J. Granwehr).

1090-7807/$ - see front matter © 2007 Elsevier Inc. All rights reserved.
doi:10.1016/j.jmr.2007.05.011

tate magic angle spinning, the polarization step and the solid-state NMR experiment were done at the same temperature, slightly above the boiling point of nitrogen [6].

While DNP processes are well understood from a thermodynamic point of view [7], further work is necessary to obtain a complete quantitative picture of the quantum-mechanical mechanisms. Since several processes are interlinked [8], further insight can be obtained by matching theoretical models to a complete set of experimental data. Apart from time constants describing relaxation and buildup of nuclear polarization, it is equally important to have relaxation data for the electron spin system, preferably at conditions as closely matched to the DNP experiment as possible. However, while the mw channel in most polarizers is designed for high power, it does not provide the frequency and power stability necessary to perform EPR experiments with heterodyne detection. This would require significant additional investment in appropriately rated mw sources, amplifiers, and power supplies. On the other hand, samples for DNP experiments are not very demanding regarding the sensitivity of the EPR spectrometer: radicals in these samples usually have high concentrations on the order of 10 mM, the samples have narrow EPR lines compared to most paramagnetic metal ions, and finally DNP is frequently done at very low temperatures resulting in long relaxation times and a very high electron spin polarization, ideally close to unity, thus causing the spins to be easily saturated.

Longitudinal detection (LOD) of EPR is based on a pickup coil aligned parallel to the static magnetic field, $\mathbf{B}_0$, to measure a changing longitudinal magnetization [9]. Maximum sensitivity is obtained with LOD if a periodic modulation of the longitudinal magnetization is induced and the signal is detected using a resonant circuit tuned to the modulation frequency [10]. However, an untuned circuit may be more robust and less prone to artifacts if the signal is high enough [11]. In the most commonly used experimental protocol, an amplitude modulated mw field is applied, and detection is done at the same frequency [12]. A different implementation uses two double-locked mw sources and detection at the difference frequency [13]. By sweeping B_0, the absorption spectrum is recorded rather than its first derivative. Alternatively, it was shown that if the mw resonator has a broad enough bandwidth, or no resonator is used at all, it is also possible to work at a static field and sweep the mw frequency [14]. Using a dissolution DNP setup that is based on a superconducting magnet with a fixed field, frequency swept EPR would not only be significantly simpler to implement since no additional sweep coils are required, but would also allow the direct comparison of the results from the EPR experiment with the DNP polarization enhancement as a function of the mw frequency for a given mw source.

LOD uses independent and well-isolated circuits for excitation and detection, with frequencies that are usually at least three orders of magnitude apart from each other. Therefore a low frequency signal can be detected while simultaneously irradiating the sample with a high-power mw field [15]. This has made it possible to measure very short relaxation times [16,17]. Using independent and uncoupled encoding and detection circuits also permits optimization of each for a different target property. For example, the mw channel could be designed for high mw power, whilst the detector could be optimized for a wide bandwidth, high sensitivity, or robustness against sample fluctuations [18].

LOD has been shown to work for a wide range of excitation and modulation frequencies. Excitation has been done at frequencies ranging from about 70 MHz [14] up to 75 GHz [19]. Modulation frequencies were typically tens to hundreds of kHz, but values up to 30 MHz have been used [20]. Since the detection circuit is working only at audio frequencies (AF) or radio frequencies (RF), it is much simpler to set up than the common heterodyne EPR detectors working at the same mw frequency as used for excitation.

In the following sections, we show how EPR capabilities can be incorporated into a dissolution DNP polarizer with minimal modifications to the instrument. We demonstrate that by using longitudinal detection at W-band (94 GHz), the absorption and first derivative EPR spectra of free radicals in a glassy matrix can both be measured. Furthermore, a technique is presented in which low-power pulse bursts are employed to measure the polarization in pump–probe experiments such as saturation-recovery and electron–electron double resonance (ELDOR) experiments. Finally, it is shown how the transient magnetization can be recorded as it approaches its steady-state, using a time-resolved measurement of the signal during an amplitude modulated excitation.

2. Instrumentation

The experimental setup, shown schematically in Fig. 1, can be divided into four more or less independent subunits: sample environment control and monitoring, which includes the magnet, the variable temperature insert (VTI), and the temperature control unit; the microwave arm; the mw shaping unit; and the detector. These subunits are discussed separately in the following sections.

2.1. Magnet and control unit

The polarizer is based on the same general layout as presented and described in more detail in [21]. The magnet (Oxford Instruments, Abingdon, UK) has a field of 3.35 T, corresponding to an electron spin Larmor frequency of 94 GHz. Since the 5 G line is inside the magnet casing, most electronic equipment could be placed directly next to the magnet. A manually operated needle valve is used to control transfer of liquid He from the main dewar of the magnet into the VTI.

Through the bore of the VTI either a sample holder for a dissolution DNP experiment or a diagnostic probe like the one described later can be inserted. The lower end of

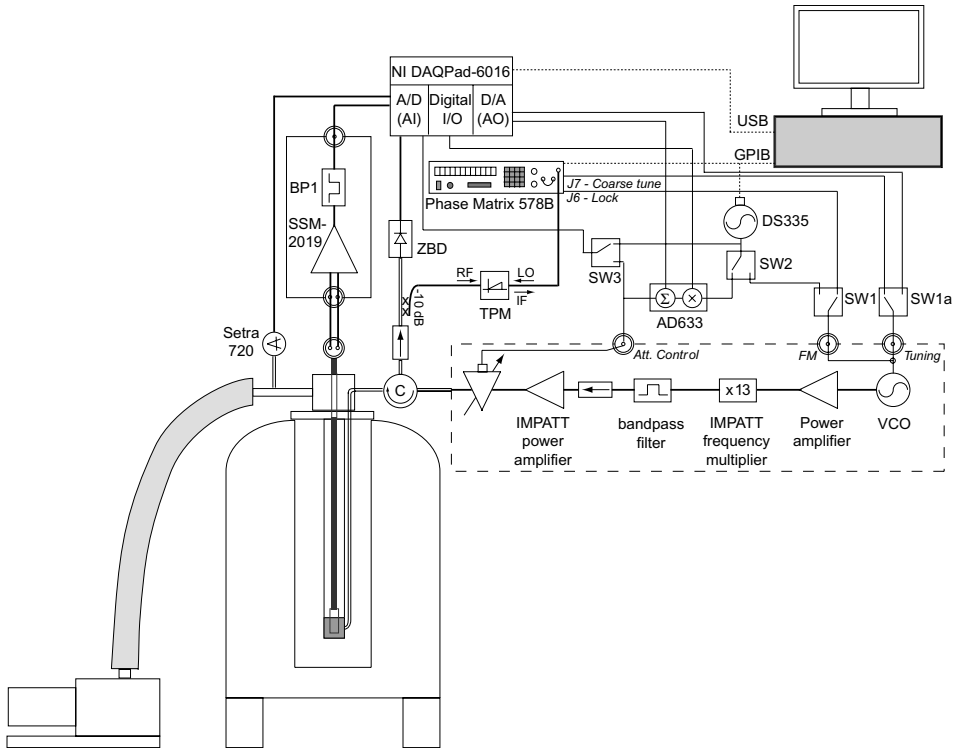

Fig. 1. Overall setup of the DNP polarizer. The dashed box represents the ELVA-1 mw source. The switches are only for illustration purposes.

the VTI is formed by a mw shield made of brass with a circular, non-adjustable iris through which the mw radiation is coupled in. A circular waveguide leads from the mw shield to a flange on the outside of the magnet for connecting the mw source.

The temperature in the VTI was reduced below the boiling point of liquid He by pumping on the He bath using a rotary vane pump (model DUO 65 M, Pfeiffer Vacuum, Asslar, Germany). This pump induced significant vibrations in the whole setup, causing a high level of noise at frequencies below about 1 kHz.

Various sensors are used to control the state of the system. On the side of the brass mw shield, a resistive Allan-Bradley temperature sensor is mounted. A vacuum transducer (model 720, Setra Systems Inc., Boxborough, MA) is used to measure the He pressure, from which the temperature can be derived. At the pump outlet, a flow meter calibrated for He with a maximum capacity of 10 l/min (model F-111B-5K0-AAD-22-V, Bronkhorst, Ruurlo, Holland) was installed to measure changes in the He boil-off rate for various heat loads in the system, for example the sample insert, probes, or the exposure of a sample to mw radiation. The He level inside the magnet bore is measured with a capacitive sensor (Oxford Instruments, Abingdon, UK) mounted at the outside of the VTI. This sensor is read out using a capacitance-to-digital converter (AD7746, Analog Devices, Norwood, MA).

An external analog-digital/digital-analog device (NI DAQPad-6016, National Instruments, Austin, TX), connected to the host computer by USB, was used to read out the various sensors. The control program was written in LabView (Version 7.1, National Instruments, Austin, TX).

2.2. Microwave arm

The microwave source (Model VCOM-10, ELVA-1, St. Petersburg, Russia) is a simplified version of the frequency source described in [22], providing 200 mW of continuous power at 94 GHz. It can be swept through a 650 MHz range by applying an external control voltage (0–10 V) to either one of the two inputs for frequency control: one intended to set the frequency (*Tuning*) and one to apply a frequency modulation (*FM*). The source is based on a voltage-controlled oscillator (VCO) providing a 7.23 GHz base frequency, which is then amplified, followed by an IMPATT frequency multiplier (13×) and an IMPATT mm-wave power amplifier. Its frequency stability largely depends on the stability of the VCO. The internal VCO of the VCOM-10 was used, but an external frequency source could be used for improved stability if necessary [23]. Finally, a voltage-controlled variable attenuator (0–55 dB) with a switching time of 25 μs is used to adjust the output power to the desired level. Variable attenuators are usually much slower than PIN switches, but the power level can be user-defined to match the optimum conditions for a certain experiment, and arbitrary waveforms can be generated within the limit of the rise time of the attenuator. Fig. 2a shows the mw output power in response to a square-wave excitation at different frequencies, ν_M. Note

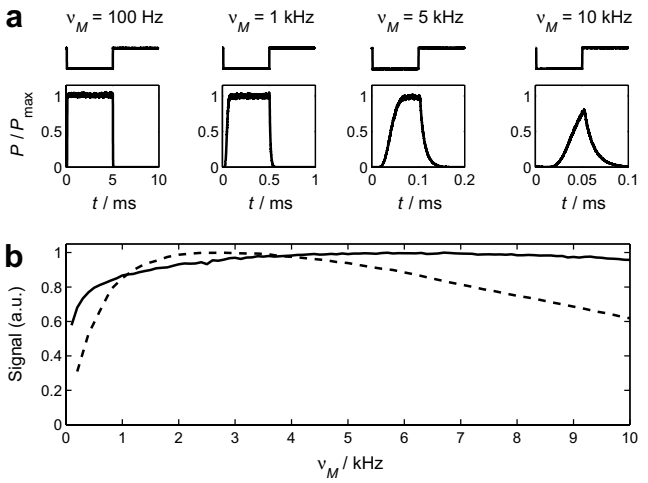

Fig. 2. Effect of changing the amplitude modulation frequency ν_M in LOD EPR experiments. (a) Reflected power, P, normalized to its maximum value, P_{max}, at different modulation frequencies. The switching of the attenuator control voltage is shown above each panel. (b) Induced signal as a function of ν_M from 15 mM trityl (solid line) and 18 mM TEMPO (dashed line), both in 1:1 water/glycerol, at 11 K. The mw frequency was kept constant at the position of maximum signal of the respective absorption EPR spectrum. Each signal is normalized to its maximum value. The influence of the analog filters used in the detector was removed numerically.

that the frequency at which the mw amplitude can be modulated is eventually limited by a delay of about 15 μs in the response of the attenuator to the switching off of the attenuating voltage. The rise of the mw power is best described by a 10–90% rise time of 30 μs. Switching on the attenuating voltage causes a delay of only 2 μs and the resulting decay of the mw power is described well by a time constant of about 10 μs.

A mw frequency counter (model 578B, equipped with frequency extension to 110 GHz, Phase Matrix Inc., San Jose, CA) is used to monitor and, if desired, lock the output frequency of the mw source. The frequency counter can be controlled and read out using GPIB. Since the internal clock of the frequency counter is more stable than the internal VCO of the mw source, this provides a convenient way not just to stabilize, but also to adjust the output frequency of the mw source. However, locking to a new frequency is relatively slow (typically on the order of several hundred milliseconds). Therefore, this option is only suitable for experiments that are performed at constant frequency, or for slow processes such as the recording of the NMR signal enhancement of the target nucleus as a function of irradiation frequency, where the same irradiation frequency is usually used for several minutes [21]. By reconnecting the cables to the *Tuning* and the *FM* input of the mw source (indicated by switches SW1 and SW1a in Fig. 1), either the 578B or an analog output (AO) of the DAQPad-6016 can be selected to control the mw frequency.

A zero-bias detector (ZBD) is used as an additional monitoring device to measure the mw power (ZBD-10/200, ELVA-1, St. Petersburg, Russia). Since it is rated up to an input power of 200 mW, it could be connected directly to the output of the frequency source.

The mw source was connected to the VTI via a circulator (model CR-10/94/1, ELVA-1, St. Petersburg, Russia). The reflected power, which is commonly large if no resonators or mw cavities are used to accommodate the sample, was then analyzed using the ZBD and the frequency counter. The two devices were connected to a −10 dB directional coupler: the ZBD to its high-power output, and the frequency counter via a two-port mixer (TPM) to its low-power output. Furthermore an isolator was inserted to suppress reflection of mw power back into the source.

2.3. Microwave control unit

Experiments were performed either in continuous wave (cw) or in low-power pulse mode. In cw mode, a continuous modulated waveform was applied to the *Attenuator control* or the *FM* inputs of the VCOM-10 source for amplitude or frequency modulated experiments, respectively. The waveform was generated using an arbitrary function generator (AFG) capable of generating sine and square waves at adjustable frequencies and amplitudes (SRS DS335, Stanford Research Systems, Sunnyvale, CA). The AFG was controlled via GPIB. The waveform was also fed into an analog input (AI) of the DAQPad-6016 as a reference to numerically demodulate the measured signal. This was necessary since the start of an acquisition at different mw frequency values was not synchronized with the waveform generated by the AFG, which was running in continuous mode.

To enable low-power pulse experiments, an AD633 analog multiplier (Analog Devices, Norwood, MA) was used to shape the modulated waveform generated by the AFG and at the same time enable DC pulses to attenuate the mw power for certain periods of time. This was implemented by multiplying the output of the AFG with the signal from a digital out line from the DAQPad. The second AO line from the DAQPad was connected to the summing input of the AD633. The output of the AD633 was then connected to the *Attenuator control* input of the VCOM-10. With this configuration, arbitrary DC pulses could be generated and, furthermore, a pulse-train could be applied for detection. The waveform used for excitation was also fed into an analog input of the DAQPad to enable phase sensitive detection. By starting detection somewhat earlier than the modulated waveform in the case of transient detection, one could get an accurate timing of the beginning of the detection pulses. The first AO line was connected to the *Tuning* input of the VCOM-10 to allow adjustment of the mw frequency as well as frequency jumps in the ELDOR experiments.

2.4. Detector

Detection was done with a pair of coils made of enameled copper wire wound in Helmholtz configuration. To avoid shielding the access of the mw to the sample, the

gap between the coils has to be at least as wide as the cutoff width for the mw frequency used in the experiment (for 94 GHz, a window of at least 1.6 mm diameter is required). Our probe had a gap of 3 mm between the two spools, each of which had 400 windings. The diameter of the wire could be kept small (0.15 mm) since experiments were carried out at very low temperatures. The bore of the detection head accommodated short, 5 mm diameter tubes for a sample volume of about 35 μl in the gap of the coil. The coil mounting and sample holder was made of PTFE; its longitudinal profile is shown in Fig. 3. The detection head was mounted at the end of a stainless steel tube with a length of about 90 cm and an outer diameter of 6 mm. This tube also served as a shield for the two leads of the coil to the connector on the outside. To minimize the heat load as well as the resistance of the coil, wires with progressively increasing thickness were used to connect the coil with the vacuum tight, SMA-type RF connector on the outside of the probe. The shield of the SMA connector was kept floating with respect to ground potential, therefore the coil could be connected directly in differential mode to an instrumentation amplifier [24]. Since the detection frequencies used in this experiment were in the audio range, an integrated microphone preamplifier (SSM2019, Analog Devices, Norwood, MA) with a low noise figure of $1\ \mathrm{nV}/\sqrt{\mathrm{Hz}}$ was used. At the output of the preamplifier, a passive band-pass filter (BP1), with a high-pass cut-off frequency of 160 Hz and a low-pass cutoff frequency of 68 kHz, was added to avoid saturating the analog-digital converter (ADC) and to filter out noise above the Nyquist frequency due to the limited sampling rate of the ADC. The signal was digitized using one of the AI channels of the DAQPad-6016. Sampling rates of up to 200 kHz were possible if only a single detection channel was used, decreasing to 100 kHz if the reference waveform was recorded simultaneously with the signal. To reduce the amount of data to be stored, the digitized transients were processed on the host computer to retain only the amplitude and phase of the frequency components of interest, which were primarily the modulation frequency and its higher harmonics. Alternatively, it was also possible to record the whole stream of data for post-processing.

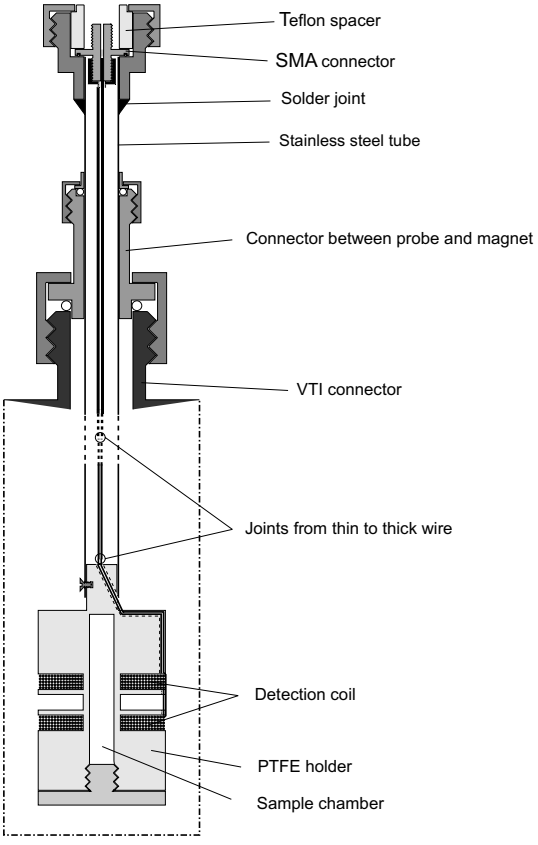

Fig. 3. LOD EPR detection probe. The head of the probe is drawn at a larger scale than the connectors. The dash-dotted line indicates the VTI into which the probe is inserted.

3. Sensitivity

Only a simplified discussion of the sensitivity achievable with LOD detection is given here. An accurate description would have to take into account the relaxation behavior of a particular sample, including the influence of spin or spectral diffusion and the orientation dependence of the electron spin relaxation rates [25]. Furthermore, the sensitivity also depends on experimental parameters such as the excitation scheme, mw power, modulation amplitude and frequency, and the duty cycle of the mw irradiation. More detailed discussions covering various situations can be found in the literature [12,13,16,20,26,27]. The present discussion gives a reasonable estimate of signal scaling with respect to different experimental and instrumental parameters representing conditions that are typical for dissolution DNP experiments.

3.1. Signal

A generic approach to describe the evolution of the signal-inducing longitudinal magnetization, $M_z(t)$, or rather its first temporal derivative, $s(t) \propto \mathrm{d}M_z(t)/\mathrm{d}t$, is to assume a periodic change of the external conditions, *e.g.* switching on and off a resonant mw field, and the subsequent relaxation of M_z towards the respective steady-state for each condition. If the mw radiation is switched periodically with a frequency ν_M, the signal will finally reach an oscillatory steady-state. This signal contains a dominant spectral component at frequency ν_M that is proportional to M_z, whose amplitude can be measured with narrow bandwidth detection. For an order-of-magnitude calculation, we assume the validity of the Bloch equations and a homogeneous spectrum with a single line to describe the magnetization. Furthermore, at low temperatures of a few Kelvin, the longitudinal relaxation time, T_1, of radicals commonly used for DNP is on the order of a second, while the transverse relaxation time, T_2, is usually fairly resistant to temperature changes [28]. On the timescale of $1/\nu_\mathrm{M}$, transverse magnetization, M_x, M_y, will dephase almost immediately,

i.e. $T_2 \ll \nu_M^{-1}$, because of the low modulation frequencies. This allows a calculation of the longitudinal magnetization $M_z(t)$ and an estimation of the sensitivity of LOD experiments as a function of time t, using a simplified set of Bloch equations which assume that $M_x(t)$, $M_y(t) \approx 0$. The rate of change of longitudinal magnetization becomes

$$\frac{dM_z}{dt} = -\frac{\omega_1^2 T_2 M_z}{1+\Omega_S^2 T_2^2} - \frac{M_z - M_0}{T_1}. \quad (1)$$

M_0 is the equilibrium magnetization of the unperturbed spins, ω_1 is the amplitude of the mw field in angular frequency units, and Ω_S is the frequency offset of the mw field. It is assumed for the sake of simplicity that the spins are exposed to a square-modulated mw field and that they have reached their oscillatory steady-state, meaning that each time the mw field is turned on, M_z changes by an equal amount but with opposite sign compared to the half-period when the mw field is turned off. If it is further assumed that $\nu_M^{-1} \ll T_1$, the exponential decay can be expanded and only the linear component retained. The transient of M_z is then a triangular waveform, and its signal-inducing first derivative is a square wave whose Fourier series is well known. To calculate the mean value of the longitudinal magnetization in the oscillatory steady-state, M_z^{ss}, the rate of change of M_z with and without mw irradiation are equated with opposite signs,

$$-\frac{\omega_1^2 T_2 M_z^{ss}}{1+\Omega_S^2 T_2^2} - \frac{M_z^{ss} - M_0}{T_1} = \frac{M_z^{ss} - M_0}{T_1}, \quad (2)$$

yielding

$$M_z^{ss} = M_0 \frac{1}{1+\frac{1}{2}\frac{\omega_1^2 T_1 T_2}{1+\Omega_S^2 T_2^2}}. \quad (3)$$

The amplitude of the signal-inducing square wave is now given by

$$\frac{dM_z^{ss}}{dt} = -\frac{M_z^{ss} - M_0}{T_1} = \frac{M_0}{2T_1}\frac{\omega_1^2 T_1 T_2}{1+\Omega_S^2 T_2^2 + \omega_1^2 T_1 T_2/2}. \quad (4)$$

It is independent of ν_M, therefore the signal does not show a dependence on the amplitude modulation frequency. However, as soon as the assumption of a triangular waveform is not justified any more, the signal decreases. If ν_M is reduced such that $\nu_M^{-1} \gg T_1$, the course of the magnetization can be approximated by a square wave modulation, whose first derivative is a succession of delta functions with a very low spectral component at ν_M, thus the signal becomes very small. In practice, a moderate increase of the signal with ν_M is typically observed until it finally reaches a plateau. If ν_M is increased until its period is on the order of the response time of the mw attenuator, the mw field does not get fully modulated any more, and the signal decreases again. Another important factor is the signal dependence on the mw power. Far below saturation, the signal is proportional to $\omega_1^2 T_2$, whilst close to saturation, the signal approaches a value proportional to $1/T_1$. Both cases are illustrated in Fig. 2b, which shows the signal induced in the detector as a function of ν_M from a 15 mM trityl and an 18 mM TEMPO sample. The two data sets were recorded at 11 K with identical instrumental settings. The same mw power was used, with mw irradiation at the respective maximum of each spectrum. The pump was turned off to reduce low-frequency noise. Both signals increase at low values of ν_M, where $\nu_M^{-1} \geqslant T_1$. The trityl signal saturates more strongly than the TEMPO signal: it levels off towards a maximum despite the deviation from the square modulation and the reduction of the mw field amplitude at high ν_M, shown in Fig. 2a. The TEMPO signal, which is more difficult to saturate, reaches a maximum at $\nu_M \approx 2.6$ kHz and then continually decreases with increasing ν_M. However, it is obvious for both samples that the signal does not increase proportionally to ν_M, as would be expected for inductive detection if the amplitude of the excitation were independent of ν_M.

By comparing the amplitude of the signal induced by the modulated longitudinal magnetization as described by Eq. (4) with the hypothetical signal, S_0, induced if a magnetization M_0 were fully sinusoidally modulated with frequency $\nu_M = \omega_M/2\pi$ in the absence of relaxation [15],

$$\frac{S^{ss}}{S_0} = \frac{2}{\pi\omega_M T_1}\frac{\omega_1^2 T_1 T_2}{1+\Omega_S^2 T_2^2 + \omega_1^2 T_1 T_2/2} \quad (5)$$

is obtained. Since typical values of ν_M are on the order of a few kHz, while T_1 is on the order of a second, it is clear that the signal in such an LOD experiment is caused by only a small fraction of the available magnetization. Fig. 4a shows the response of a homogeneous spin system to a square-wave modulated mw field, and Fig. 4b shows the relative signal intensity. The spin system is initially at equilibrium, and the mw irradiation is switched on at time $t = 0.1$ s. The dashed line in Fig. 4b represents the signal intensity in the oscillatory steady-state after the amplitude modulated mw field had been turned on for sufficiently long, as obtained with Eq. (5).

This discussion is only qualitative, since Eq. (4) was derived for homogeneous lines, while most of the samples of interest show inhomogeneously broadened EPR lines. An extension of the analytical derivation to inhomogeneous lines is possible, but spectral diffusion would need to be considered as well for samples with very long T_1 values. This is beyond the scope of the current study.

3.2. Noise processes

In an experiment with AF detection, various noise processes can be present. First of all, there is the usual thermal electronic noise of the detector with a root mean square (rms) noise amplitude of $\sigma_n = \sqrt{4kT\Delta\nu R}$, where k is the Boltzmann constant, T is the temperature, $\Delta\nu$ is the detection bandwidth, and R is the resistance of the coil. Due to the low temperature on the order of typically 1.5 K and the correspondingly low R even when thin wire is used, σ_n is

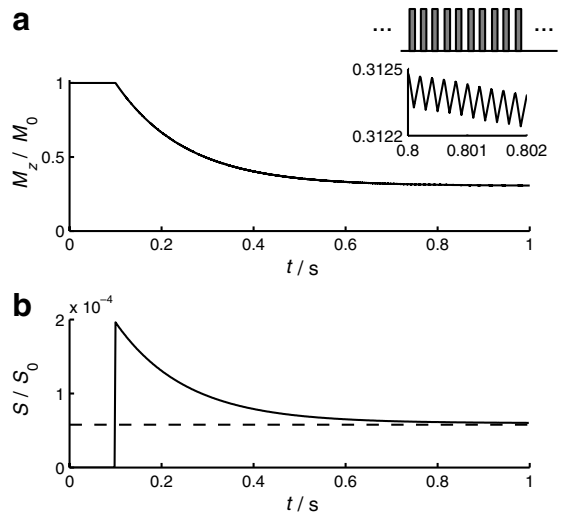

Fig. 4. Effect of a train of mw pulses on a homogeneous spin system that is initially at equilibrium. The simulation was performed using the Bloch equations, assuming $T_1 = 0.5$ s, $T_2 = 10$ μs, and $\omega_1 = 1000\ s^{-1}$. The modulation frequency was $\nu_M = 5$ kHz. (a) Transient of the longitudinal magnetization. The mw irradiation is turned on at $t = 0.1$ s. The inset shows an enlargement of a 2 ms interval (bottom) along with the position of the mw pulses (top). (b) Normalized signal induced in an untuned coil oriented parallel to B_0. The dashed line marks the signal intensity in the oscillatory steady-state.

rather low. One can get an estimate for this noise contribution of $\sigma_n/\Delta\nu \approx 5\ \mathrm{pV}/\sqrt{\mathrm{Hz}}$, where $R = 1\ \Omega$ was assumed. This value, if amplified with a gain of 1000, is on the same order as the usual noise figure of an AF preamplifier, which is typically on the order of a few $\mathrm{nV}/\sqrt{\mathrm{Hz}}$. Another noise process, which is usually less straightforward to quantify, is environmental noise. Contributions include harmonics of the power-line frequency, $1/f$-noise, or electronic and, in our case especially important, mechanical noise from devices in the vicinity of the spectrometer.

4. Excitation–detection schemes

For optimum sensitivity with LOD, excitation schemes are required that induce a periodic change of M_z. Signal detection can then be done using lock-in detection, either with a dedicated device or a transient detector and subsequent post-processing of the data.

4.1. Amplitude-modulated CW EPR

The simplest excitation scheme makes use of a periodic amplitude modulation of the mw field at a frequency ν_M. This induces a modulation of the longitudinal spin magnetization at ν_M and its higher harmonics [26]. An absorption EPR spectrum is obtained, and not its first derivative as in conventional cw EPR spectroscopy. Since no narrowband mw resonator is used in our DNP polarizer, it is possible to record EPR spectra by sweeping the mw frequency instead of the B_0 field as is common in EPR spectroscopy. The absence of a resonator with high quality factor, Q, is offset partly by the relatively high mw power of 200 mW available at 94 GHz, which still provides a reasonably strong ω_1. Furthermore, the special case of radicals at very low temperatures that is of interest in DNP experiments only requires low ω_1 values to avoid saturation of the EPR transition and the associated broadening of the EPR spectrum. The sweep width of the mw source is the same as is available in the DNP experiment, therefore the whole spectral range of interest is covered. Fig. 5a shows an absorption EPR spectrum of 15 mM trityl in a 1:1 water/glycerol glassy matrix at 11 K, obtained by modulating the amplitude of the mw field with a frequency of 10 kHz. The experimental signal-to-noise ratio (SNR) was 675, with the noise characterized by its rms amplitude.

4.2. Frequency-modulated CW EPR

To simplify the comparability of the LOD spectrum with cw EPR spectra, it is desirable to have a variation of the experiment that directly provides the first derivative of the spectrum, since numerical derivation of the absorption spectrum is usually only possible with concomitant losses in sensitivity [29]. With LOD, modulation of B_0 does not work very well since the modulated field component points in the same direction as the magnetization that induces the signal, thereby causing a huge offset in the detected signal which would saturate the receiver. However, the analogous experiment to a sweep and simultaneous modulation of B_0 would be a sweep and modulation of the mw frequency [30,31]. Such a scheme is feasible with little effort by directly modulating the control voltage of the mw source. Fig. 5b shows the first derivative spectrum of the trityl sample, obtained with a modulation frequency of 10 kHz and a modulation amplitude of 3.4 MHz. Using the peak–peak signal amplitude, the SNR was 700.

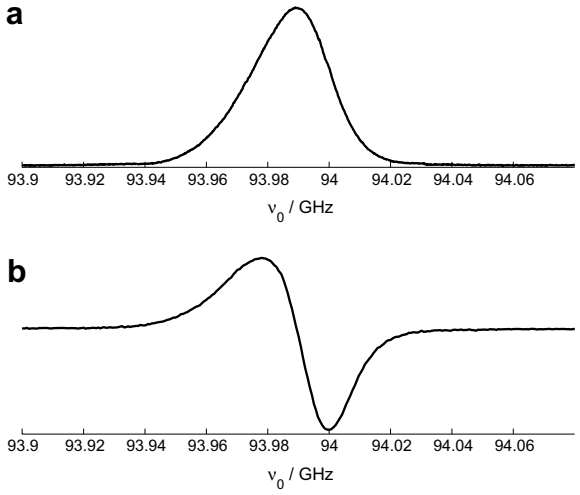

Fig. 5. LOD EPR spectrum of 15 mM trityl in 1:1 water/glycerol at 11 K. The signal at each frequency position was recorded for 1 s. (a) Absorption spectrum, obtained with amplitude modulation of the mw field. (b) First derivative spectrum, obtained by modulating the mw frequency.

The requirements for optimum performance of frequency modulated (FM) experiments are similar to a conventional cw EPR experiment: the modulation amplitude as well as the modulation frequency should be smaller than the linewidth to avoid distorted lineshapes and sidebands [31,32], and the mw amplitude should be low enough to avoid saturation.

A meaningful sensitivity comparison between the AM and the FM spectra can be obtained by performing pseudo-modulation to the AM spectrum with the same modulation amplitude as was used to record the FM spectrum [33]. In this example, the signal-to-noise ratio of the FM experiment was a factor of 2.5 better than in the pseudo-modulated AM experiment.

4.3. Low-power pulse-train detection

The signal during amplitude modulated mw irradiation is proportional to the instantaneous longitudinal magnetization. If the detection time, t_d, is reduced to a value that is short compared to the time constant at which the magnetization approaches its oscillatory steady-state value, it is possible to use a detection module at well-defined times to measure the evolution of M_z following a preparation and evolution period [17]. The simplest implementation of this scheme is to apply only a single detection pulse. However, this may not be sensitive enough considering the low mw power available and correspondingly slow change of M_z upon mw irradiation. A train of low-power mw pulses with length $0.5\,\nu_M^{-1}$ and repetition time ν_M^{-1} induces a change of M_z with an enhanced spectral component at ν_M, whose amplitude can then be obtained from a Fourier transform of the signal transient.

It is not possible to perform pulse EPR experiments with transient evolution of the transverse spin magnetization because of the low mw power and the relatively high bandwidth of the mw source, but pump–probe experiments, where only spin polarization is affected during the pump period, are feasible. The simplest of these experiments is the measurement of T_1 by saturation-recovery, where a transition is irradiated long enough for it to become saturated. This scheme is shown in Fig. 6a. Following an adjustable recovery time, t_1, the longitudinal magnetization is measured using a pulse-train. Repeating this experiment with different values of t_1, the relaxation of the magnetization towards its equilibrium value is recorded point by point. Fig. 6b shows the saturation recovery signal of a frozen solution of 5 mM TEMPO in 1:1 water/glycerol, recorded at the spectral position with maximum absorption signal. The detection time was set to $t_d = 50$ ms, corresponding to the spacing between the data points along t_1, and $T_1 = 0.31$ s was obtained.

4.4. The low-power ELDOR experiment

A potentially important parameter to know for a quantitative understanding of DNP processes is spectral diffusion. This can be quantified using an electron-electron double resonance (ELDOR) pump–probe experiment [8]. Taking advantage of the low Q of our mw shield that does not require careful tuning or frequency locking, it is possible to saturate the sample at one frequency, ω_S, and use low-power pulse-train detection to measure the influence of this saturation pulse at a different frequency ω_d (Fig. 6a). In the absence of any spectral diffusion, a difference in signal intensity should only be observed within a frequency range corresponding to the homogeneous linewidth of the sample, while spectral diffusion should broaden the hole burnt by the saturation pulse. As in the saturation recovery experiment, it is important to keep the duration of the detection pulse-train shorter than T_1 of the electron spins. Fig. 6c shows an ELDOR experiment using a sample of 18 mM TEMPO. The ELDOR spectrum almost reflects the EPR spectrum, which indicates a very strong spectral diffusion of this sample.

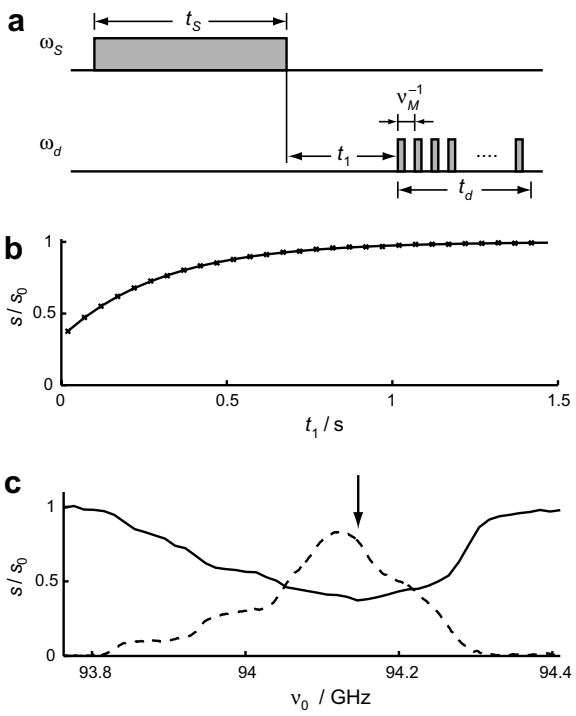

Fig. 6. (a) Generic pulse sequence of a pump–probe EPR experiment with low-power pulse-train detection. The pump frequency, ω_S, is identical to the probe frequency, ω_d, in the saturation-recovery experiment, while the mw frequency is switched at the end of the pump cycle in the ELDOR experiment. (b) Saturation recovery experiment of 5 mM TEMPO in 1:1 water/glycerol at 1.55 K. (c) ELDOR experiment of 18 mM TEMPO in 1:1 water/glycerol at 1.55 K. The pump frequency was varied across the whole spectrum, while the probe frequency was kept constant (indicated with an arrow). The solid line shows the ELDOR curve, while the dashed line shows the absorption EPR spectrum of the same sample as a reference.

4.5. Transient measurement of M_z

If the equilibration of M_z after switching on the mw pulse-train is of interest, it is possible to transiently record

the data and perform a time-resolved spectral analysis. The temporal evolution of $M_z(t)$ is obtained by piecewise Fourier transformation of the transient signal, $s(t)$. The maximum time resolution of such an experiment is given by $1/\nu_M$, whilst the sensitivity can be improved at the expense of resolution by increasing the time used to calculate each data point. This scheme is illustrated in Fig. 4, in which the response of a homogeneous spin system to a train of on-resonant mw pulses is shown.

In experiments with continuous mw irradiation and changing the mw frequency in a stepwise manner, the longitudinal magnetization is usually already close to its equilibrium value at the beginning of each acquisition. If instead a recycle delay, t_r, is introduced, during which the mw field is turned off, M_z is allowed to relax back towards its equilibrium value before each new data-point of the EPR spectrum is recorded. If t_r is significantly longer than T_1, the signal at the beginning of the acquisition is proportional to the equilibrium magnetization of the on-resonant spins, and it decays towards a saturation value during the course of the detection. Such a time-resolved experiment provides not only the unsaturated and saturated EPR spectrum if the same data set is measured at different mw frequencies across the whole spectrum, but intermediate values are also obtained that show how the spectrum evolves from equilibrium to saturation. Fig. 7 shows the result of such a time-resolved experiment with a frozen solution of 5 mM TEMPO at 1.55 K. Fig. 7a shows the EPR spectrum of TEMPO at the beginning and at the end of the irradiation. It can be seen that saturation with the available mw power is not complete. By the end of the irradiation, the signal at the center of the spectrum is still about 25% of the intensity at the beginning. Fig. 7b shows the evolution of the signal at the center of the spectrum as a function of time. Other than in the model calculation of Fig. 4b, the decay is not mono-exponential: at the beginning it decays rapidly for about 50 ms, followed by an almost linear decay towards its equilibrium value. This indicates the importance of spectral diffusion when such a result is to be analyzed quantitatively.

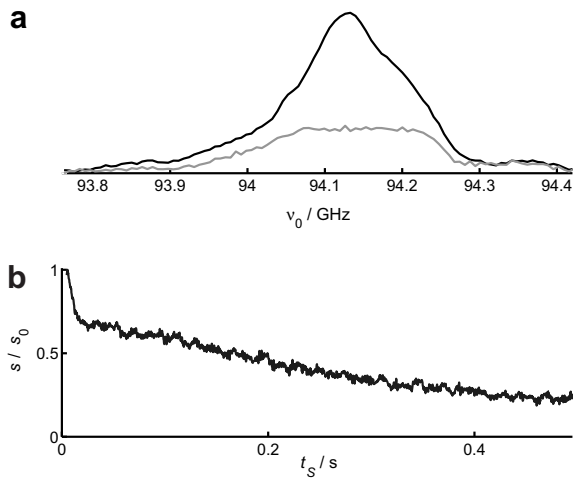

Fig. 7. Transient detection of the LOD EPR signal after switching on an amplitude modulated mw field. A sample of 5 mM TEMPO in 1:1 water/glycerol at 1.55 K was used. (a) EPR spectra at the beginning of the irradiation (black) and after an irradiation time of 0.5 s (gray). (b) Transient of the longitudinal magnetization following the switching on of an amplitude modulated mw field with a frequency of 94.153 GHz.

5. Conclusions

The feasibility of EPR detection, using an unstabilized mw source, that can be implemented as an add-on to a dissolution DNP polarizer has been presented. This can be achieved at low cost with only minimal modifications to the polarizer setup. No expensive mw parts are needed in addition to the components already used for the DNP experiment. It is a specific solution tailored to be used in a low-temperature DNP polarizer, where radicals with long relaxation times at high concentrations are used. This setup enables measurement of the DNP enhancement and the EPR spectrum in the same environment, with the same imperfections, which allows a better comparison between the two experiments. For example, experiments can be performed with the same mw power and at the same temperature, therefore identical saturation levels are possible in both experiments without demanding calibrations. Furthermore, the same frequency range is available for the DNP and the EPR experiments. As a possible future improvement to further minimize differences in the conditions between DNP enhancement and EPR experiments, the probe could be extended to also include the NMR coil for the enhancement measurements.

The feasibility of EPR detection with an AF insert, using a coil oriented parallel to the static magnetic field, and a microphone preamplifier as the only dedicated hardware, has been demonstrated. Detecting in this frequency range reduces the requirements regarding mw power losses in the mw arm, and no tuning or adjustment of the mw coupling is necessary. Nonetheless, it is desirable to reduce losses to a minimum in order to maximize the available mw power. By careful selection of the detection frequency, the influence of environmental noise can be reduced significantly without compromising the sensitivity. Since the detection frequency with LOD is determined by the modulation frequency rather than the carrier frequency of the mw field, a high frequency stability of the mw field is not needed.

Because only a mw shield, but no resonator or resonant cavity, is used in our dissolution DNP setup, performing a frequency sweep at constant B_0 field is possible. It was shown that by either modulating the amplitude or the frequency of the mw field, experiments were possible in absorption or first derivative mode, respectively.

In addition to experiments with continuous excitation and detection, it is possible to perform low-power pulse experiments with the same setup. Detection was done with a train of pulses spaced by the inverse of the detection frequency. The duration of this pulse-train had to be shorter than the lifetime of the processes that were being investigated. This allowed a saturation recovery experiment to

be performed in order to measure T_1 of the radical. Furthermore, it was possible to switch the mw frequency during an experiment, which allowed the study of spectral diffusion in an ELDOR experiment.

For quality control of the sample, the ability to measure the EPR spectrum of the radicals with the same instrument as is used for DNP can be advantageous, especially if a radical is difficult to dissolve, or if unstable radicals are being used which tend to react or decay, for example, due to exposure to light or oxygen. Furthermore, the availability of these techniques within one instrument greatly simplifies the acquisition of data for a large variety of radicals, which is a prerequisite for the development of more quantitative models to describe the mechanisms of the DNP process in the solid state.

6. Experimental

Experiments were done with solutions of either 2,2,6,6-tetramethylpiperidin-1-oxyl (TEMPO; Sigma–Aldrich, Co Ltd, Dorset, UK) or Tris{8-carboxyl-2,2,6,6-tetra[2-(1-hydroxyethyl)]-benzo(1,2-*d*:4,5-*d*′)bis(1,3)dithiole-4-yl}methyl sodium (trityl; supplied by Oxford Instruments Molecular Biotools Ltd, Abingdon, UK) radicals, dissolved in a glass-forming solution of water/glycerol (50:50). The sample concentrations were 5 and 18 mM for the TEMPO, and 15 mM for the trityl.

The mw source described in this article covers a frequency range of 93.76–94.41 GHz. If not stated otherwise, experiments were performed at a modulation frequency $\nu_M = 4.2$ kHz. Each data point in experiments with continuous detection was recorded for 1 s and then processed on the host computer before the data were written to disk.

Experiments were performed at either 11.7 K or 1.55 K: 11.7 K is the temperature of the system without liquid He in the VTI, and 1.55 K is the base temperature whilst pumping on liquid He. The higher of the two temperatures requires that sample and sample holder are allowed to thermally equilibrate for about 20 min before an experiment can be started. At the lower temperature, the VTI is immersed in liquid He, and a superfluid He film forms that quickly cools the sample.

Acknowledgments

We thank Ian Thexton and Jeffrey Smith for machining various probe parts, Rob Slade from Oxford Instruments for sharing his experience in DNP polarizer design with us, Rob Hunter and Graham Smith from the University of St. Andrews for explaining many details of high-frequency microwave instrumentation, and Brett Haywood, Jonathan McMaster, Paul Glover, John Owers-Bradley, and A.J. Perez Linde for helpful discussions. This work was supported by EPSRC and by Oxford Instruments Molecular Biotools Ltd. J.G. gratefully acknowledges a Sir Peter Mansfield Fellowship from the University of Nottingham.

References

[1] J. Ardenkjær-Larsen, B. Fridlund, A. Gram, G. Hansson, L. Hansson, M. Lerche, R. Servin, M. Thaning, K. Golman, Increase in signal-to-noise ratio of >10,000 times in liquid-state NMR, Proc. Natl. Acad. Sci. USA 100 (2003) 10158–10163.

[2] R. Wind, M. Duijvestijn, C. van der Lugt, A. Manenschijn, J. Vriend, Applications of dynamic nuclear polarization in ^{13}C NMR in solids, Prog. Nucl. Magn. Reson. Spectrosc. 17 (1985) 33–67.

[3] K. Golman, R. in 't Zandt, M. Thaning, Real-time metabolic imaging, Proc. Natl. Acad. Sci. USA 103 (2006) 11270–11275.

[4] C.-G. Joo, K.-N. Hu, J. Bryant, R. Griffin, In situ temperature jump high-frequency dynamic nuclear polarization experiments: enhanced sensitivity in liquid-state NMR spectroscopy, J. Am. Chem. Soc. 128 (2006) 9428–9432.

[5] C. Joye, R. Griffin, M. Hornstein, K.-N. Hu, K. Kreischer, M. Rosay, M. Shapiro, J. Sirigiri, R. Temkin, P. Woskov, Operational characteristics of a 14-W 140-GHz gyrotron for dynamic nuclear polarization, IEEE Trans. Plasma Sci. 34 (2006) 518–523.

[6] V. Bajaj, C. Farrar, M. Hornstein, I. Mastovsky, J. Vieregg, J. Bryant, B. Eléna, K. Kreischer, R. Temkin, R. Griffin, Dynamic nuclear polarization at 9 T using a novel 250 GHz gyrotron microwave source, J. Magn. Reson. 160 (2003) 85–90.

[7] A. Abragam, M. Goldman, Principles of dynamic nuclear polarization, Rep. Prog. Phys. 41 (1978) 395–467.

[8] C. Farrar, D. Hall, G. Gerfen, S. Inati, R. Griffin, Mechanisms of dynamic nuclear polarization in high magnetic field, J. Chem. Phys. 114 (2001) 4922–4933.

[9] G. Whitfield, A. Redfield, Paramagnetic resonance detection along the polarizing field direction, Phys. Rev. 106 (1957) 290–918.

[10] A. Schweiger, R. Ernst, Pulsed ESR with longitudinal detection. A novel recording technique, J. Magn. Reson. 77 (1988) 512–523.

[11] N. Bloembergen, R. Damon, Relaxation effects in ferromagnetic resonance, Phys. Rev. 85 (1952) 699.

[12] J. Hervé, J. Pescia, Mesure du temps de relaxation T_1 par modulation du champ radiofréquence H_1 et détection de la variation d'aimantation selon le champ directeur, C. R. Acad. Sci. Paris 251 (1960) 665–667.

[13] F. Chiarini, M. Martinelli, L. Pardi, S. Santucci, Electron-spin double resonance by longitudinal detection: line shape and many-quantum transitions, Phys. Rev. B 12 (1975) 847–852.

[14] H. Yokoyama, T. Sato, H. Ohya, H. Kamada, Longitudinally detected ESR magnetometer for wide-range measurements of low fields, J. Magn. Reson. 150 (2001) 194–197.

[15] J. Granwehr, J. Forrer, A. Schweiger, Longitudinally detected EPR: improved instrumentation and new pulse schemes, J. Magn. Reson. 151 (2001) 78–84.

[16] V. Atsarkin, V. Demidov, G. Vasneva, Electron-spin-lattice relaxation in $GdBa_2Cu_3O_{6+x}$, Phys. Rev. B 52 (1995) 1290–1296.

[17] J. Granwehr, A. Schweiger, Measurement of spin-lattice relaxation times with longitudinal detection, Appl. Magn. Reson. 20 (2001) 137–150.

[18] I. Nicholson, F. Robb, D. Lurie, Imaging paramagnetic species using radiofrequency longitudinally detected ESR (LODESR imaging), J. Magn. Reson. B 104 (1994) 284–288.

[19] F. Murányi, F. Simon, F. Fülöp, A. Jánossy, A longitudinally detected high-field ESR spectrometer for the measurement of spin–lattice relaxation times, J. Magn. Reson. 167 (2004) 221–227.

[20] J. Pescia, La mesure du temps de relaxation spin-réseau très courts, Ann. Phys. 10 (1965) 389–407.

[21] J. Wolber, F. Ellner, B. Fridlund, A. Gram, H. Jóhannesson, G. Hansson, L. Hansson, M. Lerche, S. Månsson, R. Servin, M. Thaning, K. Golman, J. Ardenkjær-Larsen, Generating highly polarized nuclear spins in solution using dynamic nuclear polarization, Nucl. Instrum. Meth. A 526 (2004) 173–181.

[22] I. Gromov, V. Krymov, P. Manikandan, D. Arieli, D. Goldfarb, A W-band pulsed ENDOR spectrometer: setup and

application to transition metal centers, J. Magn. Reson. 139 (1999) 8–17.
[23] W. Hofbauer, K. Earle, C. Dunnam, J. Moscicki, J. Freed, High-power 95 GHz pulsed electron spin resonance spectrometer, Rev. Sci. Instrum. 75 (2004) 1194–1208.
[24] P. Horowitz, W. Hill, The Art of Electronics, 2nd edition., Cambridge University Press, Cambridge, 1989.
[25] J.-L. Du, G. Eaton, S. Eaton, Temperature, orientation, and solvent dependence of electron spin–lattice relaxation rates for nitroxyl radicals in glassy solvents and doped solids, J. Magn. Reson. A 115 (1995) 213–221.
[26] J. Davies, On the longitudinal magnetization of a spin system subjected to double magnetic resonance, Solid State Commun. 20 (1976) 433–435.
[27] M. Martinelli, L. Pardi, C. Pinzino, S. Santucci, Electron-spin double resonance by longitudinal detection. II. Signal dependence on relaxation times, Phys. Rev. B 16 (1977) 164–169.
[28] A. Fielding, P. Carl, G. Eaton, S. Eaton, Multifrequency EPR of four triarylmethyl radicals, Appl. Magn. Reson. 28 (2005) 231–238.
[29] A. Schweiger, G. Jeschke, Principles of Pulse Electron Paramagnetic Resonance, Oxford University Press, Oxford, 2001.
[30] H. Hirata, T. Kuyama, M. Ono, Y. Shimoyama, Detection of electron paramagnetic resonance absorption using frequency modulation, J. Magn. Reson. 164 (2003) 233–241.
[31] M. Kälin, I. Gromov, A. Schweiger, The continuous wave electron paramagnetic resonance experiment revisited, J. Magn. Reson. 160 (2003) 166–182.
[32] C. Poole, Electron Spin Resonance—A Comprehensive Treatise on Experimental Techniques, second ed., John Wiley & Sons, New York, 1983.
[33] J. Hyde, M. Pasenkiewicz-Gierula, A. Jesmanowicz, W. Antholine, Pseudo field modulation in EPR spectroscopy, Appl. Magn. Reson. 1 (1990) 483–496.